Journal of Engineering Science *Vol. XXXIII, no. 2 (2026), pp. 32 - 45*
Fascicle *Industrial Engineering* *ISSN 2587-3474*
Topic *Materials Science and New Technologies* *eISSN 2587-3482*

https://doi.org/10.52326/jes.utm.2026.33(2).03
UDC 621.383.51:620.92

ZnTe – BASED OF PEROVSKITE SOLAR CELLS WITH INVERTED PLANAR ARHITECTURE

Mihail Popa *, ORCID: 0009-0007-7903-3946

Technical University of Moldova, 168 Stefan cel Mare blvd., MD2004, Chisinau, Republic of Moldova
* Corresponding author: Mihail Popa, *mihail.popa@fiz.utm.md*

Received: 04.14.2026
Accepted: 05.22.2026

Abstract. This article presents applications of zinc telluride in perovskite solar cells. Devices in which the thin layer of ZnTe deposited by thermal evaporation is the only hole transport layer reached a maximum yield of about 2.14%, while those with hole transport layer consisting of PEDOT-PSS doped with ZnTe had a maximum efficiency of about 2.60%. Power conversion efficiency of approximately 7.40% was recorded in solar cells consisting of two hole transport layers, one of ZnTe and one of PEDOT-PSS. The maximum conversion yield of approximately 13.84% was recorded in devices, in which heterojunction was made from perovskite doped with ZnTe.

Keywords: *perovskite, zinc telluride, current density, voltage, fill factor, efficiency.*

Rezumat. Articolul prezintă aplicații ale telururii de zinc în celule solare cu perovskit. Dispozitivele în care stratul subțire de ZnTe depus prin evaporare termică este singurul strat de transport al găurilor au atins un randament maxim de aproximativ 2,14%, în timp ce cele cu strat de transport al găurilor constând din PEDOT-PSS dopat cu ZnTe au avut o eficiență maximă de aproximativ 2,60%. O eficiență de conversie a puterii de aproximativ 7,40% a fost înregistrată în celulele solare constând din două straturi de transport al găurilor, unul din ZnTe și unul din PEDOT-PSS. Randamentul maxim de conversie de aproximativ 13,84% a fost înregistrat în dispozitivele în care heterojoncțiunea a fost realizată din perovskit dopat cu ZnTe.

Cuvinte cheie: *perovskit, telurură de zinc, densitate de curent, tensiune, factor de umplere, eficiență.*

Abbreviations

ZnTe - Zinc telluride
ZnSe - Zinc selenide
ZnO – Zinc oxide
PEDOT-PSS – composite material where PEDOT (the conductive polymer) and PSS (polystyrene sulfonate).
$PC_{61}BM$ - [6,6]-phenyl-C_{61}-butyric acid methyl ester.
AFM - atomic force microscopy.
PCE - power conversion efficiency

1. Introduction

$A^{II}B^{VI}$ type semiconductor compounds have a wide range of optical and electrical properties and can become competitive materials in photovoltaic conversion and optoelectronic applications [1]. On the other hand, the structure and physical properties of the thin layers of these compounds greatly depend on the deposition method and the substrate temperature, the evaporation method and the deposition rate.

ZnTe is a binary semiconductor compound, type $A^{II}B^{VI}$, with the band gap average E_g = 2.26 eV at T = 300 K. Typically, zinc telluride crystallizes in cubic form (sphalerite, or "zincblende"), but can also be prepared as a hexagonal structure (wurtzite) [3].The compound, together with sulfides and selenides, belongs to the calcogenide category. In the form of thin layers it can be prepared by various methods such as thermal evaporation technique from one source [4] and two sources [5], electrodeposition [6, 7], epitaxial growth [8, 9], sputtering [1], molecular beam epitaxy [10], direct combination of Zn and Te in quartz ampoule [2, 11], pulsed-laser deposition [12].

Zinc telluride is an important material for photovoltaic applications. T. Tanaka et al. [13] presented the experimental results of the photovoltaic activity of the homojunction ZnTe from solar cells in which n-ZnTe layers are made by thermal diffusion of Al into p-ZnTe. W. Wang et al. [10] have grown n-ZnO/n-ZnSe/p-ZnTe structures on GaAs and GaSb and they demonstrated good rectifier diode qualities and good photovoltaic response. C. A. Wolden et al. [14] have prepared ZnTe buffer layers as posterior contact of CdTe solar cells and have significantly contributed to raising the efficiency of cells and to improving the stability of the module. N. G. Patel et al. [15] have demonstrated that the efficiency of p-ZnTe / n-CdSe type solar cells in thin layers strongly depends on the conditions of growth of the absorption layers and the window layers. P. Saikia et al. [16] have prepared ZnSe/ZnTe/CdTe/HgTe multijunction solar cells on tin oxide-coated glass substrate using the vacuum evaporation method and these structures have demonstrated the best photovoltaic parameters [2].

I believe that the ability of contemporary researchers to manufacture perovskite cells with a high filling factor is an important step towards assembling high-efficiency cells for commercial applications. Today, the number of researchers with perovskite solar cells with an efficiency of less than 15% is increasing [17]. J.Y. Jeng et al. showed solar cells similar to pervoskite $CH_3NH_3PbI_3$ / fullerene (C_{60}) planar - hybrid heterojunction with the following parameters V_{oc} = 0.60 V, J_{sc} = 10.30 mAcm^{-2}, *FF* = 0.63, *PCE* = 3.9% [18]. L. Etgar et al. reported obtaining hole conductor-free mesoscopic methylammonium lead iodide ($CH_3NH_3PbI_3$) perovskite / TiO_2 heterojunction solar cell with important photovoltaic characteristics: J_{sc} = 16.1 mA/cm^2, V_{oc} = 0.631 V, *FF* = 0.57 and *PCE* = 7.3% [19]. J.H. Im et al. have demonstrated highly efficient quantum-dot-sensitized solar cell based on perovskite $CH_3NH_3PbI_3$ with PCE = 6.54% [20]. M.M. Lee [21] presented a device with the structure FTO/TiO_2/$CH_3NH_3PbI_2Cl$/Spiro-OMeTAD/Ag and the most efficient device exhibited have photovoltaic characteristics: J_{sc} = 17.8 mAcm^{-2}, V_{oc} = 0.98 V, FF = 0.63 and η = 10.9 % [22]. N.J. Jeon et al. have discovered a solvent engineering technology for the preparation of extremely uniform perovskite layers and demonstrated a solution-processed perovskite solar cell with an energy conversion efficiency of about 16.5% [23]. Similar applications of thin layers of ZnSe, ZnTe and ZnS in perovskite solar cells have demonstrated M.E. Popa et al. [24 – 27].

Perovskite solar cells based on organic - inorganic halides [25] have aroused a special interest in research due to the increase of photovoltaic characteristics and the simpler way of preparation compared to other solar cells [28-37]. Replacing silicon with absorbent thin

layers in such devices will greatly reduce the real cost of solar cells. The objectives of this paper are to present the experimental results of the use of thin layers of ZnTe and ZnTe powder in various variants of perovskite solar cells [25].

2. Materials and Methods

The lower electrodes of the solar cell were deposited from indium tin oxide (ITO) by etching on Corning 7059 glass [25], which had been initially ultrasonically cleaned in detergent, deionized water and acetone. The ITO layer served as cathode collecting holes.

The thin layer of ZnTe was subsequently deposited in vacuum as a hole transport layer by means of thermal evaporation. The mass of ZnTe powders with a purity of about 99.999% ranged from 15 to 32 mg. Substrate temperature was T_{sub} = 300 K, vacuum pressure - about 0.96 Pa, and electric power through the evaporator process was approximately 50 A.

The thickness of the ZnSe films was measured with the MII-4 interference microscope (Linnik type), the operation of which is based on the interference of fringes of equal thickness from the surface of the layer and the surface of the support. The DRON-3 diffractometer with MoKα radiation (λ = 0.710687 Å) was used to obtain X-ray diffractograms. The surface morphology of ZnTe thin layers was characterized by AFM.

The bulk heterojonction layer [25] was prepared of 80 μl of methylammonium lead iodide solution ($MAPbI_3$ = $CH_3NH_3PbI_3$) by the spin-coating method in two stages: after the first deposition the layer was rotated at a speed of 1000 rpm for 23 seconds, followed by a second deposition and a rotation at a speed of 4000 rpm for 30 seconds. 150 μl of toluene dropped in the 13th second [24].

The $PC_{61}BM$ (= PCBM) film was used as electron transport layer. It was deposited from the solution in the argon chamber by the spin-coating method at a rotational speed of 1000 rpm for 40 s [38]. The advantages of using $PC_{61}BM$ as an electron transport layer are: layers are deposited from the solution, their thickness can be adjusted, good electron transport properties in the deposited layers and the lack of need for additional heat treatment. Energetic direction of the holes and electrons is more favorable in this configuration, electrons move to a metal with small extraction work, and the holes move to material with large extraction work. Ag electrodes were deposited by thermal evaporation in a quasi-closed volume [24].

In another variant of perovskite solar cells the PEDOT-PSS layer doped with ZnTe powder was used as the hole transport layer, and the other layers were deposited analogously as in the first variant of solar cells [27]. The concentration of the powder in the mixture varied between 1.0 and 2.0 mg/ml. This was deposited from the solution by the spin-coating method for 60s at a rotational speed of 3000 rpm. Then followed a heat treatment in air for 10 minutes at a temperature of 150^{o}C. Heat treatment time was measured with the stopwatch of a mobile phone.

The third type of perovskite solar cells had a two-layer structure (ZnTe + PEDOT-PSS) which fulfill the function of hole transport layer, and the other layers were deposited analogously as in the first variant of solar cells [25]. The ZnTe layer was deposited by thermal evaporation under conditions similar to those of the first type of solar cell, and the second layer of PEDOT-PSS was deposited by the spin-coating method under conditions similar to those of the second type of solar cells [39].

The last variant of solar cells uses as bulk heterojunction the perovskite layer $CH_3NH_3PbI_3$ doped with ZnTe powder, and the other layers were deposited similar into as in the first type of solar cells.

To measure the current density - voltage of solar cells dependencies, a closed box filled with nitrogen using simulated AM1.5G sun light was used, which was calibrated to 100 mW/cm^2 using an NREL tracking photodiode and a computer-controlled Keithley 2400 source unit [25]. The HITACHI S-3000N microscope was used for SEM measurements and the photovoltaic characteristics were measured at room temperature.

3. Results and Discussion

In Fig. 1 are presented two SEM images of a solar cell type ITO/PEDOT-PSS/$MAPbI_3$: ZnTe/$PC_{61}BM$/Ag after depositing the $PC_{61}BM$ fullerene layer. We notice that the surface of the cell is uniform, without perforations, but with some small spherical grains grown on the surface (about 3 μm in diameter) and elongated (3 to 5 μm in length) [24]. This uniform compact structure effectively blocks the recombination of charge carriers at the surface.

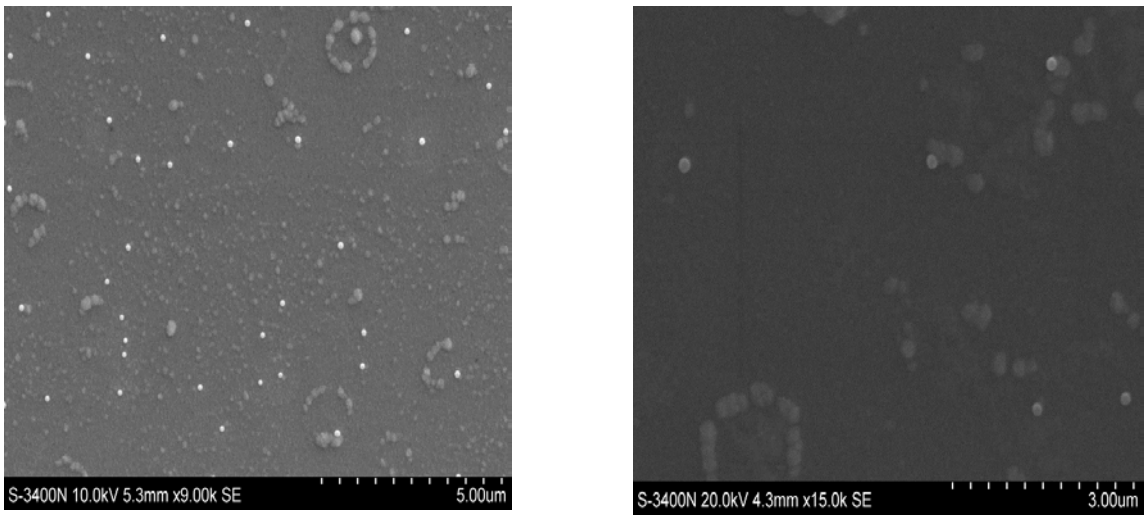

a) b)

Figure 1. The SEM images of surfaces of samples type ITO/PEDOT-PSS/$MAPbI_3$: ZnTe/$PC_{61}BM$/Ag.

Figure 2 (a) presents the schematic cross-section of the first variant of perovskite solar cells with inverted architecture described in this article, and the scheme of energy transitions in the layers of this solar cell are shown in Fig. 2 (b). Here the role of electron transport layer is fulfilled by the $PC_{61}BM$ film, and the role of hole transport layer - the ZnTe layer [25]. From this diagram we observe that the hole runs through the energy path -5.4 eV → -5.1 eV → -4.7 eV, and the electron runs through the energy path -3.9 eV → -4.3eV → -4.5 eV.

The output current of the photovoltaic cell is given by the relation [16, 40],

$$I = I_s \left[exp\left(\frac{q(V - IR_s)}{kT} \right) - 1 \right] - I_L, \quad (1)$$

where I_s and R_s are the diode saturation current and the series resistance of the respective cell. The fill factor that measures the quality of solar cells is determined by the relation [16, 40]

$$FF = \frac{I_m V_m}{I_{sc} V_{oc}}, \quad (2)$$

where I_m and V_m are the current and the voltage corresponding to the maximum power point P_{max} and I_{sc} and V_{oc} respectively short-circuit current and open-circuit voltage. An important parameter is the power conversion efficiency (*PCE*) of the solar cell, which is defined as the ratio from the output power (electricity) and the input power (the light) and can be calculated by the equation [16, 40]:

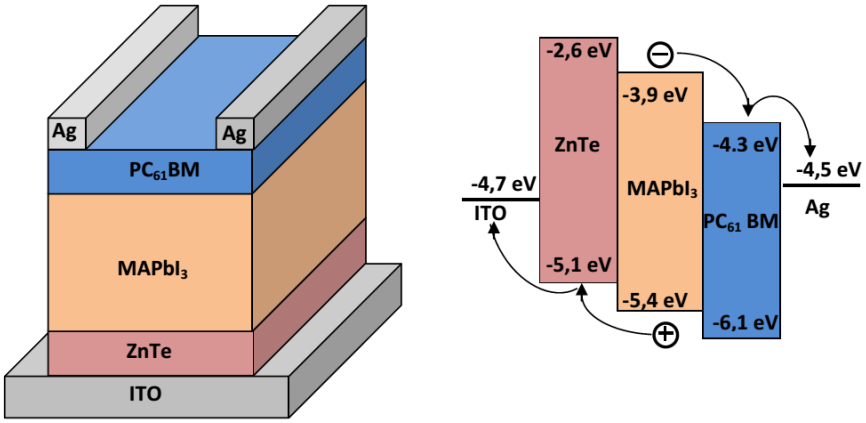

a) b)

Figure 2. (a) Device structure of first type of solar cells;
(b) The energy diagram of first type of solar cell.

$$PCE = \eta = \frac{P_{output}}{P_{input}} = FF\frac{I_{sc}V_{oc}}{P_{input}}. \quad (3)$$

Typically, the "inverted" planar structure has a V_{oc} and a high *FF*, which are indicators that this structure has favorable electrical contacts and that the charges are efficiently collected on electrodes within this structure.

The *J-U* dependencies and the photovoltaic parameters of the solar cells with the ITO/ZnTe/$MAPbI_3$/PCBM/Ag structure are presented in Fig. 3 and Table 1 [25].

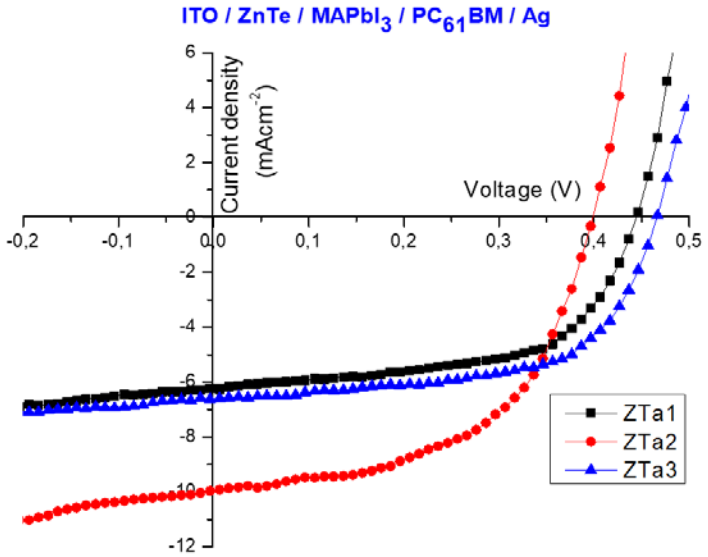

Figure 3. Current density – voltage characteristics of first type of solar cells.

The experimental curves were constructed according to the thickness of the ZnTe layer deposited on the ITO, and the photovoltaic parameters analyzed were open circuit voltage (V_{oc}), short-circuit current (J_{sc}), fill factor (*FF*) and power conversion efficiency (*PCE*). For the cell with a ZnTe layer thickness of about *d* = 20 nm, the electrical dependence ZTa1 was obtained with the following characteristics: V_{oc} = 0.44 V, J_{sc} = - 6.24 mA/cm^{-2}, *FF* = 59.48 %, *PCE* = 1.66 %. For the device with the thickness of the ZnTe layer of about *d* = 33 nm, the ZTa2 curve was obtained, in which the hysteresis of the curve increased to the value J_{sc} = - 9.98 mA/cm^{-2}, and V_{oc} decreased to 0.39 V. For the solar cell with the ZnTe layer thickness of *d* = 48 nm the ZTa3 curve was obtained, which is very close to the form of the initial *J-U* dependency ZTa1 [25].

Table 1

Photovoltaic parameters of first type of solar cells

Devices	d_{ZnTe} (nm)	U_{oc} (V)	J_{sc} (mA/cm^2)	FF (%)	PCE (%)
ZTa1	20	0.44	-6.24	59.48	1.66
ZTa2	33	0.39	-9.98	54.19	2.14
ZTa3	48	0.46	-6.62	61.14	1.88

Low values of the power conversion efficiency is probably due to mainly the small displacement of the ZnTe valence band to the perovskite valence band and probably due to low crystallinity and high roughness of the surface of the ZnTe layer. Thus, the ZnTe layer with the function of hole transporting layer did not improve charge transport, but probably created increased contact resistance.

For the best ITO/ZnTe/$MAPbI_3$/PCBM/Ag solar cell the characteristic *J-U* was measured to the forward lighting (at decrease of voltage) and reverse lighting (at increase of voltage) (Fig. 4). From Table II we notice that at reverse scanning V_{oc} decreases from 0.390 V to 0.386 V, J_{sc} decreases from 9.98 mAcm^{-2} to 9.61 mAcm^{-2}, *FF* is reduced from 54.19 % to 51.49 % and *PCE* decreases from 2.14 % up to 2.02 %.

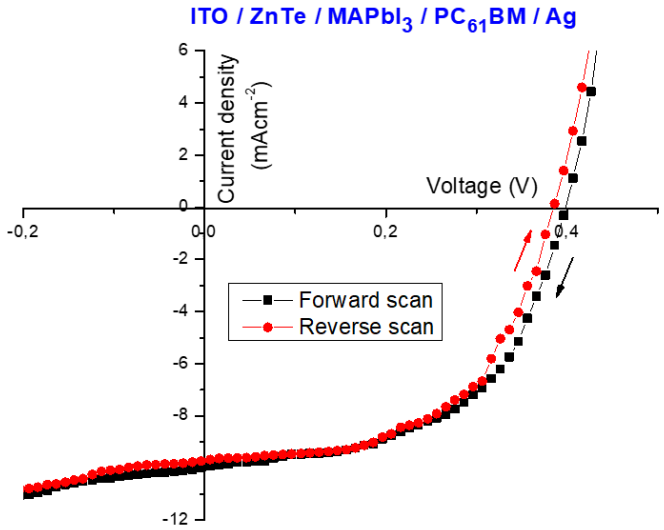

Figure 4. Forward and reverse J-U characteristics of ZTa2 device (d_{ZnTe} = 33 nm).

Table 2

Parameters of of ZTa2 solar cell (d_{ZnTe} = 33 nm) with forward and reverse scanning

Directions of scanning	U_{oc} (V)	J_{sc} (mA/cm^2)	FF (%)	PCE (%)
forward	0.390	-9.98	54.19	2.14
reverse	0.386	-9.61	51.49	2.02

The structure and morphology of a ZnTe layer deposited on the ITO electrode and the glass support was investigated. In the XRD diffractogram (Fig. 5.a) three diffraction peaks (111), (200) and (311) were identified in ASTM and ICDD data sheets for ZnTe, which demonstrates that the studied layers are polycrystalline and have a zinc blend structure with a strong orientation of the crystalites with the planes (111), (200) and (311) parallel to the surface of the support. The AFM image of the ZnTe thin layer surface is shown in Fig. 5.b. It is noted that the sample has small crystalites, grooved perpendicular to the support, in the

form of "scales" with similar dimensions (length about 0.08 - 0.1 μm, width about 0.04 - 0.06 μm). The image of Fig. 5.c demonstrates that the thickness of the ZnTe layer is about 33 nm and has a surface roughness of about 3 - 5 nm.

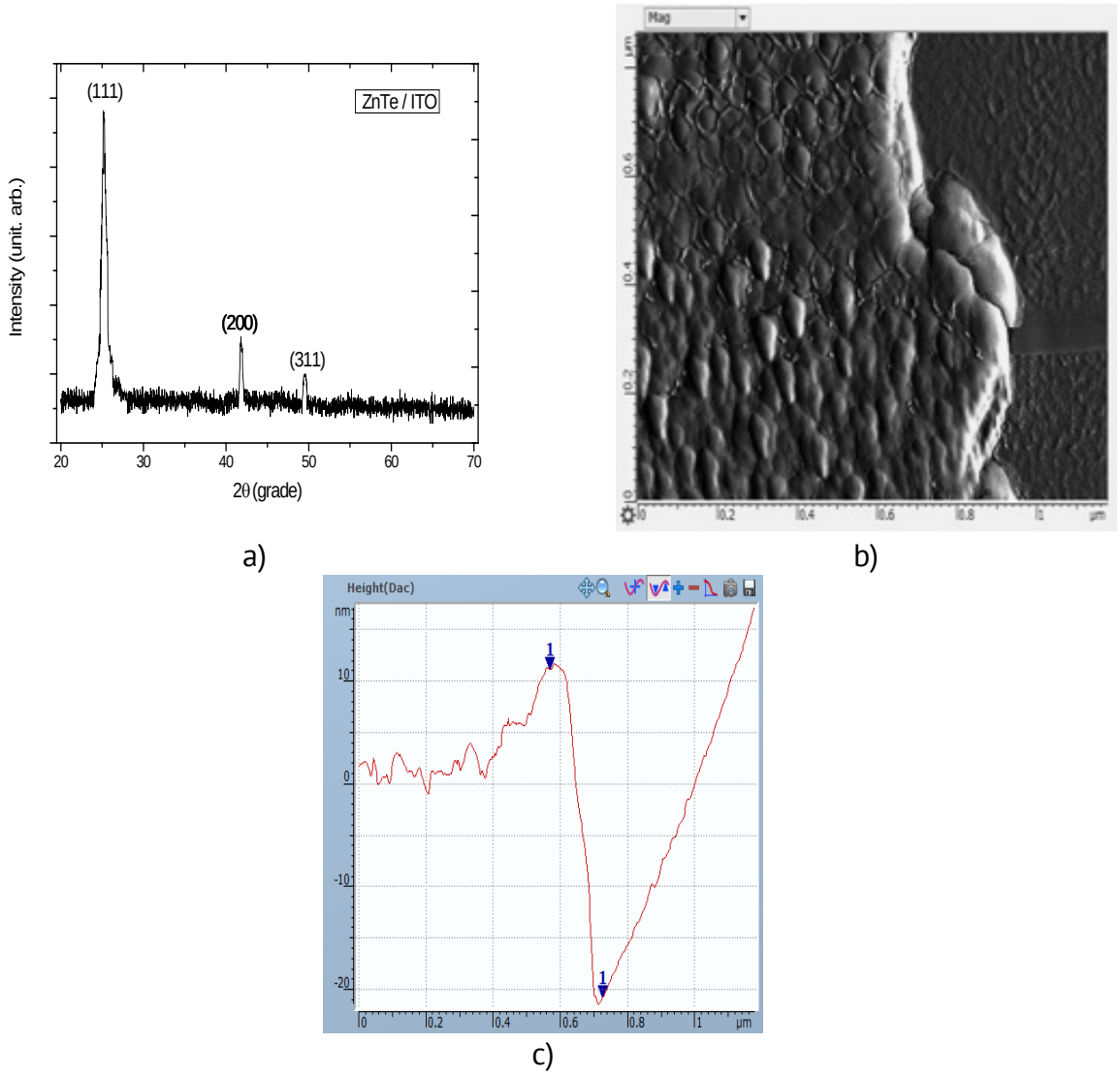

Figure 5. (a) XRD image confirming the crystalline structure of the ZnTe layer: b) AFM image of the ZnTe layer deposited on ITO/glass,c) AFM image to measure the height of ZnTe layer deposited on ITO/glass.

The modification of hole transport layer in order to increase of the power conversion efficiency of solar cells it was achieved by doping the PEDOT: PSS solution with the ZnTe powder. The concentration of the powder in the solution ranged from 1.2 - 2.0 mg/ml.

Fig. 6 presents the current density - voltage dependencies of solar cells with ITO/PEDOT-PSS: ZnTe/$MAPbI_3$/PCBM/Ag structure, and Table 3 represents the parameters of the respective cells. For the ZTb1 solar cell with the concentration n = 1.2 mg/ml of ZnTe in PEDOT-PSS, the experimental curve with the following characteristics was obtained: V_{oc} = 0.58 V, J_{sc} = - 5.64 mA/cm^2, *FF* = 43.94%, *PCE* = 1.43%. The hysteresis of the ZTb4 curves, with the concentration n = 1.8 mg/ml of ZnTe in PEDOT-PSS, increased continuously reaching the values J_{sc} = - 9.27 mA/cm^2 and V_{oc} = 0.69 V, which corresponds to the maximum value of *PCE* = 2.56 %. For solar cells with a concentration n > 1.8 mg/ml of ZnTe in PEDOT-PSS the hysteresis becomes lower than in the previous cell, and the energy efficiency decreases continuously.

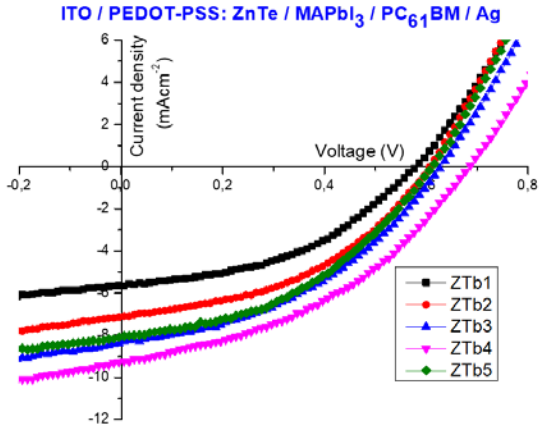

Figure 6. J-U curves of the second type of solar cells.

Table 3

Photovoltaic parameters of the second type of solar cells [25]

Devices	*n (mg/ml)*	U_{oc} *(V)*	J_{sc} *(mA/cm²)*	*FF (%)*	*PCE (%)*
ZTb1	1.2	0.58	-5.64	43.94	1.43
ZTb2	1.4	0.60	-7.14	43.32	1.88
ZTb3	1.6	0.63	-8.40	40.94	2.15
ZTb4	1.8	0.69	-9.27	40.31	2.56
ZTb5	2.0	0.62	-8.10	41.50	2.07

Fig. 7 and Table IV show small deviations in *J-U* characteristic at forward lighting (at decreasing of voltage) and reverse lighting (at increasing the voltage) of the best solar cell type ITO/PEDOT-PSS:ZnTe/$MAPbI_3$/PCBM/Ag.

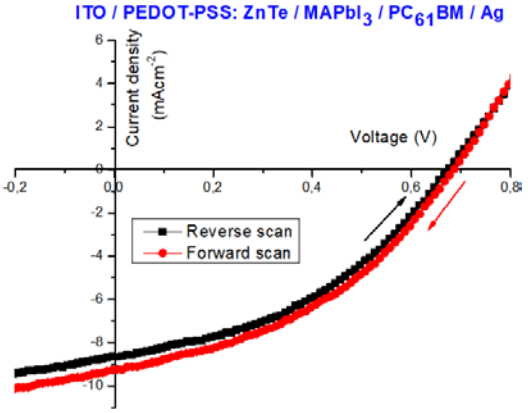

Figure 7. Forward and reverse J-U characteristics of ZTb4 device (n = 1.8 mg/ml).

Table 4

Parameters of of ZTb4 solar cell (n = 1.8 mg/ml) with forward and reverse scanning

Directions of scanning	U_{oc} *(V)*	J_{sc} *(mA/cm²)*	*FF (%)*	*PCE (%)*
forward	0.69	-9.27	40.31	2.56
reverse	0.67	-8.63	40.16	2.38

To increase the efficiency of hole transport layer a third variant of solar cells was prepared in which two layers of p-type conduction were deposited: a ZnTe film obtained by quasi-closed thermal evaporation, the thickness of which was measured after each deposition, and the second layer of PEDOT-PSS obtained by the spin-coating method.

Fig. 8 presents the most representative J-U curves of solar cells with ITO/ZnTe / PEDOT: PSS/$MAPbI_3$/PCBM/Ag structure, which were analyzed according to the thickness of the ZnTe layer deposited on the ITO, and their energy quantities are indicated in Table V. The ZTc1 solar cell has the thickness of the ZnTe layer equal to 20 nm and the characteristic current density - voltage has the following photovoltaic parameters: V_{oc} = 0.94 V, J_{sc} = 12.73 mA/cm^2, *FF* = 59.87% and *PCE* = 7.14%. The ZTc2 device with a ZnTe layer thickness of about 33 nm has a significantly higher short-circuit current value of about 19.16 mA/cm^2, and an open circuit voltage of less than 0.78 V. The hysteresis of the ZTa3 solar cell, with a ZnTe layer thickness equal to 48 nm, decreases, and the characteristic current density - voltage moves upwards, perpendicular to the current density axis. In all perovskite solar cells with ZnTe as the electron transport layer from Fig. 8 a *PCE* > 7% was obtained [25].

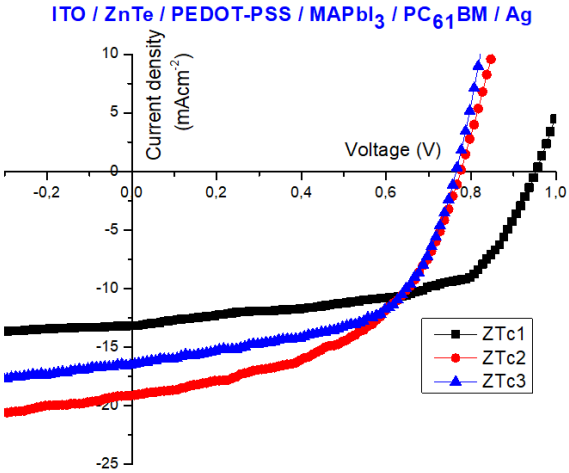

Figure 8. Current density – voltage characteristics of *the* third type of solar cells.

Table 5

Photovoltaic parameters of the third type of solar cells

Devices	d_{ZnTe} *(nm)*	U_{oc} *(V)*	J_{sc} *(mA/cm^2)*	*FF (%)*	*PCE (%)*
ZTc1	20	0.94	-12.73	59.87	7.14
ZTc2	33	0.78	-19.16	49.71	7.40
ZTc3	48	0.77	-16.52	56.38	7.14

The energy diagram of recent solar cells is shown in Fig. 9. It is noticed that this structure significantly simplifies the movement of the holes from the perovskite to the ITO electrode by making smaller jumps, in a cascade, between close energy levels (from 5.4 eV to 5.2 eV and then from 5.1 eV to 4.7 eV). This probably explains the increase in the PCE value of those cells compared to other solar cells.

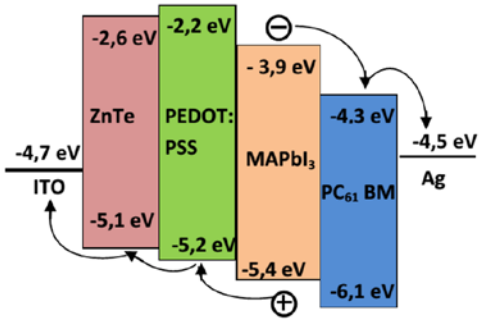

Figure 9. The energy diagram of the third type of solar cells.

J-U characteristic of ZTc2 device at reverse illumination presented a smaller hysteresisthan the forward illumination (Fig. 10). From Table 6 we note that at reverse scanning V_{oc} decreases from 0.78 V to 0.70 V, J_{sc} increases from 19.16 mAcm^{-2} to 19.63 mAcm^{-2}, *FF* decreases from 49.71 % to 48.11 % and PCE declines 7.40 % to 6.67 %.

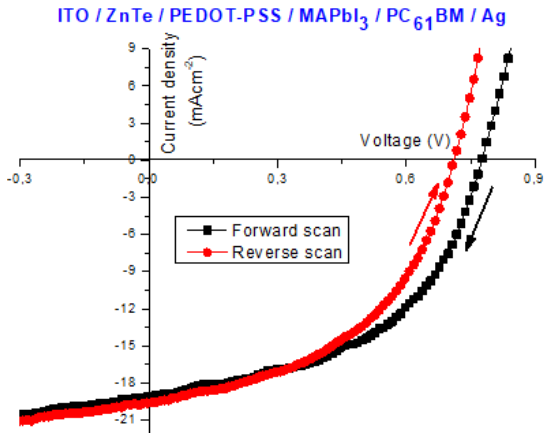

Figure 10. Forward and reverse J-U characteristics of ZTc2 device (d_{ZnTe} = 33 nm).

Table 6

Parameters of ZTc2 solar cell (d_{ZnTe} = 33 nm) with forward and reverse scanning

Directions of scanning	U_{oc} (V)	J_{sc} (mA/cm^2)	FF (%)	PCE (%)
forward	0.78	-19.16	49.71	7.40
reverse	0.70	-19.63	48.11	6.67

By doping the perovskite solution ($CH_3NH_3PbI_3$) with the ZnTe powder in the bulk heterojonction layer, the fourth variant of solar cells was obtained. In the solar cells with the best photovoltaic characteristics the concentration of the powder in the solution varied between 1.2 - 1.8 mg/ml. The mode of deposition of this layer was the same as in the case of depositing the pure layer of perovskite. Other layers-components of the solar cells were prepared analogously to the ZTal – ZTa3 samples.

The J-U dependencies of solar cells with ITO/PEDOT: PSS/$MAPbI_3$: ZnTe/PCBM/Ag structure are represented in Fig. 11, and the photovoltaic parameters of the respective solar cells are presented in Table 7. For the solar cell in which the concentration of ZnTe in $MAPbI_3$ is *n* = 1.2 mg/ml, the ZTd1 curve was obtained with the following characteristics: V_{oc} = 0.95 V, J_{sc} = 15.52 mA/cm^{-2}, *FF* = 61.56%, *PCE* = 9.05%. Increasing the concentration of ZnTe to *n* = 1.4 mg/ml it is observed that the open circuit voltage remains practically constant, and the hysteresis of the current density-voltage curve increases to the value of short-circuit current of about 24.97 mA/cm^2, and the value maximum *PCE* = 13.84%. If the concentration of ZnTe in $CH_3NH_3PbI_3$ increases even more than in the ZTd2 solar cell, the energy efficiency of the solar cells decreases continuously, because the V_{oc} and *FF* values decrease [25].

Table 7

Photovoltaic parameters of the fourth variant of solar cells

Devices	n (mg/ml)	U_{oc} (V)	J_{sc} (mA/cm^2)	FF (%)	PCE (%)
ZTd1	1.2	0.95	-15.52	61.56	9.05
ZTd2	1.4	0.95	-24.97	58.53	13.84
ZTd3	1.6	0.92	-25.97	51.92	12.36
ZTd4	1.8	0.86	-27.04	39.36	9.12

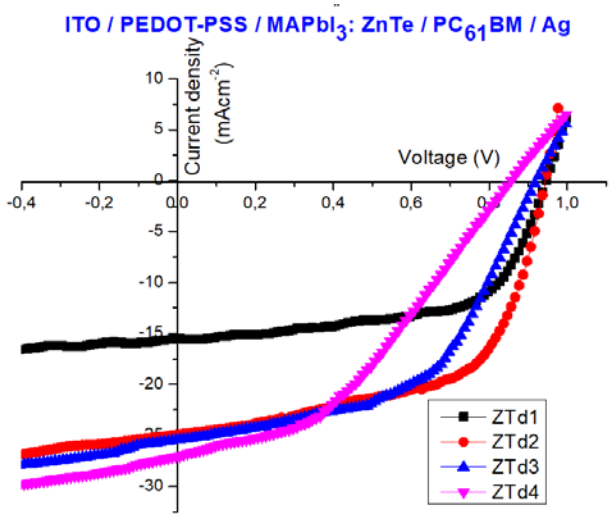

Figure 11. Current density – voltage characteristics of the fourth variant of solar cells.

Fig. 12 represents the current density - voltage dependencies for the most efficient ZTd2 solar cell. A direct scan of the solar cell the J-U dependence revealed the following parameters: V_{oc} = 0.95 V, J_{sc} = 24.97 mA/cm^2, FF = 58.53 %, PCE = 13.84 %, and at the reverse scan V_{oc} = 0.91 V, J_{sc} = 24.96 mA/cm^2 , FF = 55.38 % and PCE = 13.32 % (Table 8).

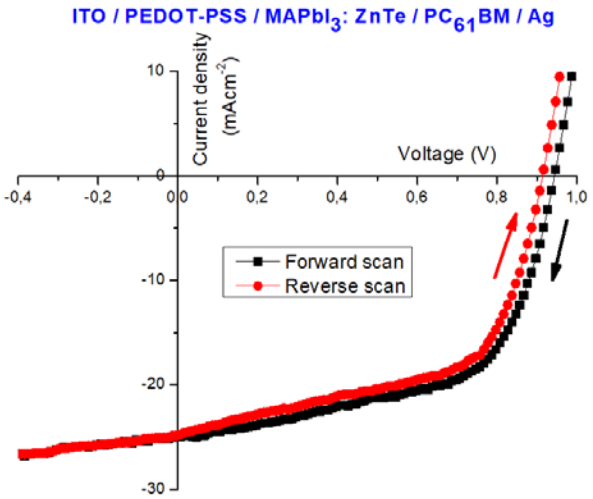

Figure 12. Forward and reverse J-U characteristics of ZTd2 device (*n = 1.8 mg/ml*).

Table 8

Parameters of ZTd2 solar cell (n = 1.8 mg/ml) with forward and reverse scane

Directions of scane	*U_{oc} (V)*	*J_{sc} (mA/cm^2)*	*FF (%)*	*PCE (%)*
forward	0.95	-24.97	58.53	13.84
reverse	0.91	-24.96	55.38	13.32

5. Conclusions

The paper demonstrated the experimental results obtained in the preparation and investigation of perovskite solar cells in which ZnTe performed the function of hole transport layer. The highest power conversion efficiency PCE ≈ 7.40% was detected in ITO/ZnTe/ PEDOT-PSS/$MAPbI_3$/PCBM/Ag devices with an open circuit voltage V_{oc} ≈ 0.777 V, a filling factor FF ≈ 0.50 and with a short-circuit current J_{sc} ≈ - 1.02 mA/cm^2. By doping perovskites with ZnTe solar cells with the structure ITO/PEDOT-PSS/$CH_3NH_3PbI_3$: ZnTe/$PC_{61}BM$/Ag were obtained with the best photovoltaic characteristics: PCE = 13.84%, V_{oc} = 0.947 V, FF = 59% and J_{sc} = - 24.97 mA/cm^2.

References

1. Bellakhder H, Debbagh F, Outzourhit A, Bennouna A, Brunel M, Ameziane E (1997) Characterization of Te/Zn/Te … multilayers deposited by RF-sputtering, Sol. Energy Mater. Sol. Cells, 45(4), 361-368. https://doi.org/10.1016/S0927-0248(96)00083-9
2. Aqili A, Ali Z, Maqsood A (2000) Optical and structural properties of two-soursed evaporated ZnTe thin films, Applied Surface Science, Vol. 167, Issues 1-2, p. 1-11 DOI: 10.1016/S0169-4332(00)00498-0
3. Haynes WM, Eds., (2011), CRC Handbook of Chemistry and Physics, 92nd ed., CRC Press.
4. Aboraia AM, Ahmad M, Abdel Wahab EA, Shokry Hassan H., Shaaban ER (2015) Structural and optical properties of ZnTe thin films induced by plasma immersion O − ion implantation. Int. J. New. Hor. Phys. 2(1), 11-20. http://dx.doi.org/10.12785/ijnhp/020103
5. Aqili A, Ali Z, Maqsood A. (2000) Optical and structural properties of two-sourced evaporated ZnTe thin films. Applied Surface Science, 167 (1-2), 1-11. DOI:10.1016/S0169-4332(00)00498-0
6. Ishizaki T, Ohtomo T (2004) Structural, optical and electrical properties of ZnTe thin films electrochemically deposited from a citric acid aqueous solution, Journal of Physics D: Applied Physics 37(2), 255-261. DOI:10.1088/0022-3727/37/2/014
7. Murali KR, Rajkumar PR, (2006) Characteristics of pulse plated ZnTe films, Journal of materials science. Materials in electronics 17(5), 393-396. DOI**:** 10.1007/s10854-006-7476-1
8. Matsumoto T, Ishida T (1984) Chemical vapor deposition of zinc chalcogenides using elemental source materials, Journal of Crystal Growth, 67(1), 135-140. DOI:10.1016/0022-0248(84)90142-8
9. Guo Q, Nada M, Ding Y, Tanaka T, Nishio M (2010) Low-temperature buffer layer effects on the quality of ZnTe epilayers grown on sapphire substrates. J. Appl. Phys., 107, 123525-1 - 123525-5. https://doi.org/10.1063/1.3452356
10. Wang W, Phillips J, Pan X. (2011). ZnO/ZnSe/ZnTe Heterojunctions for ZnTe - Based Solar Cells, J. Electron. Mater. 40(8), 1674-1678. DOI:10.1007/s11664-011-1641-x
11. Pal U, Saha S, Chaudhuri AK, Rao V, Banerjee HD (1989) Some optical properties of evaporated zinc telluride films, J. Phys. D: Appl. Phys. 22(7), 965-970. DOI:10.1088/0022-3727/22/7/014
12. Erlacher A, Ambrico M, Perna G, Schiavulli L, Ligonzo T, Jaeger H., Ullrich B, Erlacher A (2005) Absorption and photoconductivity properties of ZnTe thin films formed by pulsed-laser deposition on glass, Appl. Surf. Sci. 248(1-4), 402-405. https://doi.org/10.1016/j.apsusc.2005.03.041
13. Tanaka T, Yu KM, Stone PR, Beeman JW, Dubon OD, Reichertz LA, Kao VM, Nishio M, Walukiewicz W (2010). Demonstration of homojunction ZnTe solar cells, J. Appl. Phys., 108(2), 024502-1 – 024502-2 DOI:10.1063/1.3463421
14. Wolden CA, Abbas A, Li J, Diercks DR, Meysing DM, Ohno TR, Beach JD, Barnes TM, Walls JM (2016) The roles of ZnTe buffer layers on CdTe solar cell performance, Sol. Energy Mater. Sol. Cells, 147, 203-210. https://doi.org/10.1016/j.solmat.2015.12.019
15. Patel NG, Panchal CJ, Makhija KK, Patel PG, Patel SS (1994) Fabrication and characterization of ZnTe/CdSe thin film solar cells, Crystal Research and Technology, 29(2), 247-251. https://doi.org/10.1002/crat.2170290214
16. Saikia P, Saikia PK, Saikia (2011) Fabrication and characterization of ZnSe/ZnTe/ CdTe/ HgTe multijunction solar cell, Optoelectron. Adv. Mat. 5(3), 204-207.
17. Yella A, Heiniger LP, Gao P, Nazeeruddin MK, Gratzel M (2014) Nanocrystalline Rutile Electron Extraction Layer Enables Low-temperature Solution Processed Perovskite Photovoltaics with 13,7 Efficiency, Nanoletters, vol. 14, Issue 5, pag. 2591-2596 DOI: 10.1021/nl500399m
18. Jeng JY, Chiang YF, Lee MH, Peng SR, Guo TF, Chen P, Wen TC (2013) $CH_3NH_3PbI_3$ perovskite / fullerene planar - heterojunction hybrid solar cells, Adv. Mater., 25(27), 3727-3732 DOI: 10.1002/adma.201301327
19. Etgar L, Gao P, Xue Z, Peng Q, Chandiran AK, Liu B, Nazeeruddin MK, Grätzel M (2012) Mesoscopic $CH_3NH_3PbI_3/TiO_2$ Heterojunction Solar Cells, J. Am. Chem. Soc., 134(42), 17396. DOI: 10.1021/ja307789s
20. Im JH, Lee CR, Lee JW, Park SW, Park NG (2011) 6.5% efficient perovskite quantum-dot-sensitized solar cell, Nanoscale, 3, 4088-4093, https://doi.org/10.1039/C1NR10867K
21. Lee MM, Teuscher J, Miyasaka T, Murakami T, Snaith HJ (2012) Efficient hybrid solar cells based on mesosuperstructured organometal halide perovskites, Science, 338(6107), 643-647. DOI: 10.1126/science.1228604
22. Giorgi G, Yamaschita K, Zero-dipole molecular organic cations in mixed organic–inorganic halide perovskites: possible chemical solution for the reported anomalous hysteresis in the current–voltage curve measurements, Nanotechnology, vol. 26, Nr. 44, DOI: 10.1088/0957-4484/26/44/442001

23. Jeon NJ, Noh JH, Kim YC, Yang WS, Ryu S., Seok S.I, (2014) Solvent engineering for high-performance inorganic-organic hybrid perovskite solar cells, Nat. Mater, 13(9), 897-903. DOI: 10.1038/nmat4014
24. Popa M, Zakhidov A, Tiginyanu I (2018) Perovskite solar cells with ZnS as electron transport layer, Proceedings of Romanian Academy, series A, vol. 19, No. 4, p. 559-566. https://www.repository.utm.md/bitstream/handle/5014/10900/Proc_of_theRomanian_Academy_2018_N4_p559_566.pdf?isAllowed=y&sequence=1
25. Popa ME (2019), Applications of Chalcogenides as Hole Transport Layers and Dopants in Perovskite Solar Cells, In Proceedings of 4th International Conference on Nanotechnologies and Biomedical Engineering, September 18–21, 2019, Chisinau, Moldova, p. 177-180. https://link.springer.com/book/10.1007/978-3-030-31866-6
26. Popa ME (2019), Applications of Chalcogenides as Electron Transport Layers and Doping Materials in Perovskite Solar Cells, In Proceedings of 4th International Conference on Nanotechnologies and Biomedical Engineering, September 18–21, 2019, Chisinau, Moldova, p. 173-176 https://link.springer.com/book/10.1007/978-3-030-31866-6
27. Popa ME (2020), Current-voltage characteristics of ZnSe-based Perovskite solar cells with inverted planar architecture, Journal of Optoelectronics and Advanced Materials, vol. 22, No. 7-8, p. 371 – 378, https://joam.inoe.ro/articles/current-voltage-characteristics-of-znse-based-perovskite-s-olar-c-ells-with-inverted-planar-architecture/fulltext
28. Stranks SD, Eperon GE, Grancini G, Menelaou C, Alcocer MJP, Leijtens T, Herz LM, Petrozza A, Snaith HJ (2013) Electron-Hole Diffusion Lengths Exceeding 1 Micrometer in an Organometal Trihalide Perovskite Absorber, Science, 342 (6156), 341-344. DOI: 10.1126/science.1243982
29. Yin WJ, Shi T, Yan Y (2014) Unique properties of halide perovskites as possible origins of the superior solar cell performance, Adv. Mater., 26(27), 4653-8. DOI: 10.1002/adma.201306281
30. Yin WJ, Shi T, Yan Y (2015) Superior Photovoltaic Properties of Lead Halide Perovskites: Insights from First-Principles Theory, J. Phys. Chem. C, 119(10), p. 5253–5264 DOI:10.1021/jp512077m
31. Bidikoudi M., Stathatos E (2024) Chalcogenides in Perovskite Solar Cells with a Carbon Electrode: State of the Art and Future Prospects, Nanomaterials, 14(22), 1783. DOI: 10.3390/nano14221783
32. Wang C, Nie R, Dai Y, Tai H, Zhu B, Zhao L, Wu Y, Guo W, Seok SI (2024**)** Enhancing the Inherent Stability of Perovskite Solar Cells through Chalcogenide-Halide Combinations. Energy Environ. Sci. , 17, 1368–1386, DOI: 10.1039/D3EE03612J
33. Njema, GG, Kibet JK, (2025) A Review of Chalcogenide-Based Perovskites as the next Novel Materials: Solar Cell and Optoelectronic Applications, Catalysis and Future Perspectives, Next Nanotechnol. , 7, 100102. DOI: 10.1016/j.nxnano.2024.100102
34. Agresti A, Giacomo FD, Pescetelli S, Carlo AD (2024) Scalable Deposition Techniques for Large-Area Perovskite Photovoltaic Technology: A Multi-Perspective Review, Nano Energy, 122, 109317. DOI:10.1016/j.nanoen.2024.109317
35. Rehman UU, Sahar KUl, Mahmood K, Hussain E, Wang CM (2025) Exploring the potential of non-toxic chalcogenide based perovskite solar cells: Performance analysis and insights, Inorganic Chemistry Communications, Volume 174, Part 1, 113923 https://doi.org/10.1016/j.inoche.2025.113923
36. Shimul A I, Khan M A, Rayhan A, Ghosh A (2025), Machine Learning-Based Optimization and Performance Enhancement of $CH_3NH_3SnBr_3$ Perovskite Solar Cells with Different Charge Transport Materials Using SCAPS-1D and wxAMPS, Advansed Theory and Simulations, DOI: 10.1002/adts.202500182
37. Saadat M, Amiri O (2024), Chalcogenide perovskites for solar energy applications: The role of Sn substitution in $BaZrS_3$-based photovoltaic devices, Inorganic Chemistry Communications, 168, 112977, DOI: 10.1016/j.inoche.2024.112977
38. Wada H, Kuwayama C, Hiroshiba N, Koike K, Kawaha M, (2026) Characterization of VO_2 thin films deposited on flexible ultrathin glass via MOD, Materials Letters, Volume 403, 139374, https://doi.org/10.1016/j.matlet.2025.139374
39. Shorok E, Bedir Y, Mohy Eldin AAE (2021) Efficiency enhancement of intermediate band solar cell using front surface pyramid grating, Optical and Quantum Electronics, vol. 53, nr. 360, https://link.springer.com/article/10.1007/s11082-021-03007-6
40. Sze SM (1981) Physics of Semiconductor Devices, 2nd Ed., John Wiley and Sons, New York

Citation: Popa., M. (2026). ZnTe – Based of perovskite solar cells with inverted planar arhitecture. *Journal of Engineering Science*. 2026, 33 (2), pp. 32-45. https://doi.org/10.52326/jes.utm.2026.33(2).03.

Submission of manuscripts: jes@meridian.utm.md